AIAA 82-4080

Electrostatic Velocity Adjustment of Payloads Launched by Lunar Mass-Driver

T.A. Heppenheimer*
Center for Space Science, Fountain Valley, Calif.
David J. Ross†
Phoenix Engineering, Inc., Palo Alto, Calif.
and
Eric C. Hannah‡
Hewlett-Packard Research Laboratories, Palo Alto, Calif.

Payloads launched by lunar mass-driver do not incorporate onboard midcourse correction capability, and their trajectories must be accurately adjusted to a specified launch state. We consider electrostatic methods for this adjustment. For adjustment transverse to the flight path, we propose a cylindrical array of parallel rods surrounding the flight path, which simulate a capacitor formed from oppositely charged hemicylinders. We give a solution for the action on a spherical payload of its multiple charged rods, and present reference configurations for which the capacitance is given analytically. The transverse force is ~50 N/MV.[2] For adjustment of velocity magnitude we propose a tandem array of conducting toroids, their central holes forming a tunnel for the flight path. We treat capacitance and performance for a single charged toroid; again the longitudinal force generated is ~50 N/MV[2]. We derive a stability criterion for longitudinal adjustment. We discuss problems posed by the required high static voltages, noting breakdown mechanisms and critical voltages, effects of dust, charging of payloads, and solar wind effects. The most serious problem appears to be preventing breakdown (arcing) initiated by loose dust particles from the payloads.

I. Introduction

In recent years, the mass-driver has received attention as a means of employing the linear synchronous motor for launching payloads from the moon. Figure 1 illustrates schematically the integration of a mass-driver into a lunar launch system. Such a system provides for the industrial manufacture of payloads; their acceleration aboard "buckets" or payload carriers; the removal of launch errors; the separation of payloads from buckets; and the regenerative braking and recirculation of buckets.

The payloads are conceived[1] as spherical bodies with conducting surfaces, manufactured from lunar soil, with no onboard navigation or course-correction capability. Hence their launch accuracy depends entirely upon the fidelity with which external mechanisms can act upon them to produce a desired state vector at launch. The associated accuracy requirements are severe,[2] and launch state vectors must be regarded as corrupted by "launch noise." Previous investigators[3] have noted the need for downrange correction or removal of launch noise. They have proposed the action of static electric fields upon a payload in free flight subsequent to launch to adjust both flight direction and velocity magnitude.

However, apart from order-of-magnitude estimates indicating the utility of such fields, these previous workers have not given specific analyses or reference design concepts. In the present work we seek to address these problems. In addition we give performance estimates for reference geometries, and we note certain difficulties associated with use of high voltages.

Received Nov. 25, 1980; revision received Aug. 7, 1981.

*President. Associate Fellow AIAA.
†President.
‡Member of the Technical Staff.

II. Adjustment of Flight Direction

A. Preliminary Considerations

A transverse acceleration may be applied with a charged parallel-plate capacitor.[3] If a spherical payload of radius a is charged to potential V, and if the plate potentials are V, $-V$, and the plate separation d_p, then the force on the payload is

$$F = (8\pi\epsilon_0 a/d_p)\,V^2 = 222.53\,(a/d_p) \qquad \text{N/MV}^2 \qquad (1)$$

where ϵ_0 is the permittivity constant, 8.85415×10^{-12} in MKS units. Equation (1) defines a performance standard, to which any other configuration is compared. However, such a parallel-plate corrector is inherently capable of correction in only one direction. It is evidently of interest to consider a geometry which permits correcting fields to be applied in any transverse direction.

Such a geometry is that of Fig. 2a. The corrector is a cylindrical array of conducting rods, any of which may be electrostatically charged. The rods have radius r and length l; their surfaces are separated by clearance c. To produce a desired direction of deflection, one would charge half the rods positive and the diametrically opposite half negative, thus simulating a parallel-plate capacitor formed from two hemicylinders.

Such a geometry is studied using the method of images. In Fig. 2b, a conducting sphere of radius a is in the presence of an external point charge q. The electric field external to the sphere then is that of charge q, an image charge $-q'$, and a neutralizing chaege q' at the sphere center. If q is at distance ρ from the center, $-q'$ is at distance y:

$$y\rho = a^2 \qquad q' = qa/\rho \quad \text{C} \qquad (2)$$

If the sphere contains charge Q, the central point charge is $Q+q'$. If the sphere is grounded, the neutralizing charge q' vanishes.

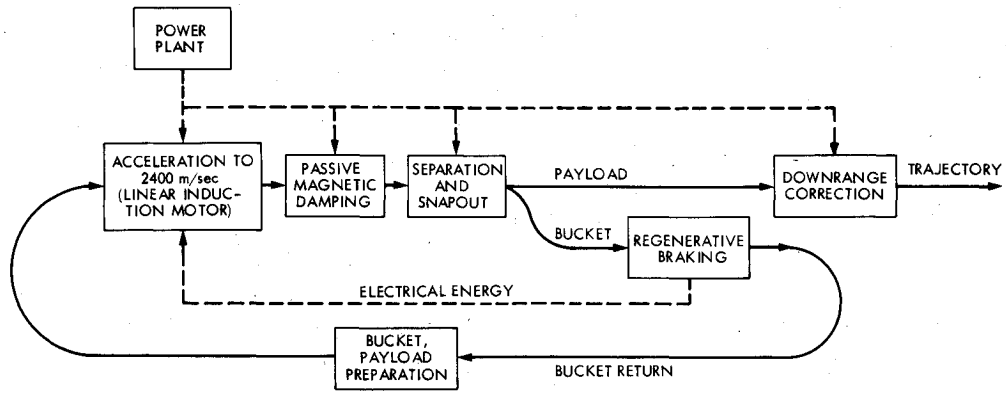

Fig. 1 Block diagram of lunar mass-driver launch system (modified from Chilton et al.).

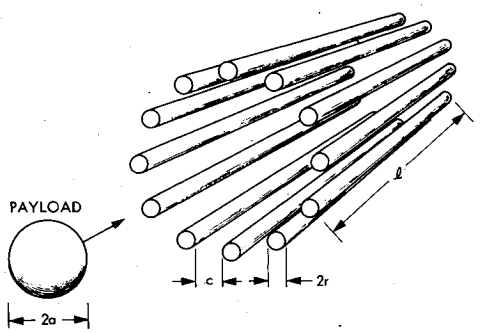

Fig. 2a Geometry of spherical payload entering a transverse corrector.

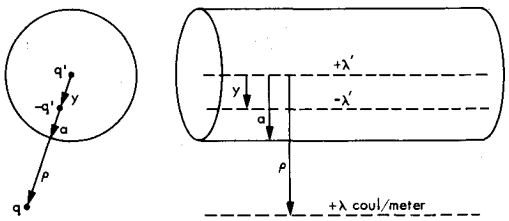

Fig. 2b Electrostatic images set up by an external point and line charge.

Also in Fig. 2b is a long conducting cylinder of radius a in the presence of an external line charge λ C/m. The associated field external to the cylinder is that of λ, an image line charge $-\lambda'$, and a central neutralizing line charge λ':

$$y\rho = a^2 \qquad \lambda' = \lambda \quad \text{C/m} \tag{3}$$

Again, if the cylinder is grounded, the neutralizing line charge λ' vanishes.

In Fig. 2a, let a single rod be charged, generating an isolated line charge λ. Figure 3a represents the associated geometry. For each $dq = \lambda dl$ in the charged rod, the image charge is $-dq'$, located distance $y(\theta)$ from the payload center:

$$dq' = a\lambda \sec\theta d\theta$$

$$y(\theta) = \frac{a^2}{r+a+c}\cos\theta \equiv \frac{a^2}{R}\cos\theta \tag{4}$$

and $R = r+a+c$. The second of Eqs. (4) is a circle of radius $a^2/2R$ passing through the sphere center and coplanar with the line charge. The force due to the charged rod upon the payload, their mutual clearance being c, is[4]

$$F = \frac{\lambda}{\pi\epsilon_0}\left[\frac{Q}{2R} - \lambda\left(\frac{a}{R}\right)^2 \frac{\sin^{-1}(a/R)}{(1-(a/R)^2)^{1/2}}\right] \quad \text{N} \tag{5}$$

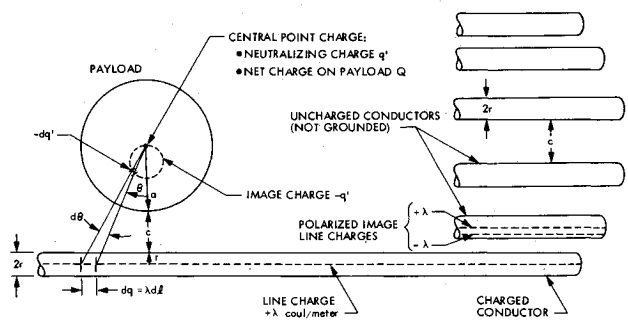

Fig. 3a Geometry of a charged sphere acted upon by a charged linear conductor.

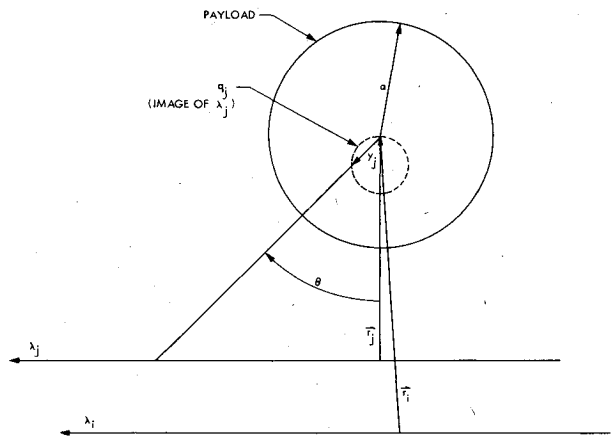

Fig. 3b Charged sphere acted upon by two line charges; for clarity only the single image charge loop q_j is shown.

Q is the net charge on the sphere. By convention F is positive when repulsive (oriented away from the rod).

B. Theory of Transverse Correction

Consider the action on the payload of multiple lines of charge. The method of images permits an exact treatment. Each line charge redistributes the charge upon the sphere, the charge redistribution being represented as an array of virtual (image) charges inside the sphere. Any such array then is acted upon by each line charge, including the one that set it up. These effects then add by superposition. For any two line charges λ_i, λ_j the situation is as in Fig. 3b. Line j has an image charge q_j within the sphere which is acted upon by the electric field of line i, and vectors $\vec{r}_i, \vec{r}_j$ extend to the center of the sphere respectively from lines i,j. The image of an element of line j in the sphere has magnitude dq_j and is located distance $y_j(\theta)$ from the center, as in Eqs. (4):

$$dq_j(\theta) = a\lambda_j \sec\theta d\theta \qquad y_j(\theta) = (a^2/r_j)\cos\theta \tag{6}$$

where θ is in Fig. 3b. Also a neutralizing charge $-dq_j(\theta)$ appears at the sphere center. The force produced on this induced charge pair by line i is

$$d\vec{F}_{ij} = \frac{\lambda_i}{2\pi\epsilon_0}\left(\frac{\vec{r}_i}{r_i^2} - \frac{\vec{Y}}{Y^2}\right) a\lambda_j \sec\theta d\theta \tag{7}$$

where

$$\vec{Y} = \vec{r}_i - (y_j/r_j)\vec{r}_j\cos\theta \tag{8}$$

and $\vec{Y}$ is the vector from line i to the image charge element $dq_j(\theta)$.

We have, for example, $r_i^2 = \vec{r}_i \cdot \vec{r}_i, \hat{r}_i = \vec{r}_i/r_i$. Hence Eqs. (6-8) give $\vec{F}_{ij}$, the force of line i on the image and neutralizing charges due to line j:

$$\vec{F}_{ij} = \frac{\lambda_i\lambda_j a\alpha_{ij}}{2\pi\epsilon_0 r_i}\int_{-1}^{1}\frac{\vec{R}_{ij}}{\vec{R}_{ij}\cdot\vec{R}_{ij}}dx \quad \text{N} \tag{9}$$

where $x = \sin\theta$, $\alpha_{ij} = a^2/r_i r_j$, and

$$\vec{R}_{ij} = (\alpha_{ij} - 2\hat{r}_i\cdot\hat{r}_j)\hat{r}_i + \hat{r}_j - \alpha_{ij}x^2\hat{r}_i$$

$$\vec{R}_{ij}\cdot\vec{R}_{ij} = (\alpha_{ij}^2 - 2\alpha_{ij}(\hat{r}_i\cdot\hat{r}_j) + 1) + 2\alpha_{ij}[(\hat{r}_i\cdot\hat{r}_j) - \alpha_{ij}]x^2 + \alpha_{ij}^2x^4 \tag{10}$$

Equations (9,10) hold also for line j acting on its own image charge. The definite integral then is evaluated using partial fractions:

$$\vec{F}_{ij} = \frac{\lambda_i\lambda_j a\alpha_{ij}}{2\pi\epsilon_0 r_i b_{ij}}\left\{\frac{(\alpha_{ij} - 2\cos\phi_{ij} - b_{ij})\hat{r}_i + \hat{r}_j}{c_{ij}} \times\left[\tan^{-1}\left(\frac{2\alpha_{ij}+d_{ij}}{c_{ij}}\right) + \tan^{-1}\left(\frac{2\alpha_{ij}-d_{ij}}{c_{ij}}\right)\right] + \frac{(\alpha_{ij} - 2\cos\phi_{ij} + b_{ij})\hat{r}_i + \hat{r}_j}{2d_{ij}}\ln\left(\frac{\alpha_{ij}+b_{ij}+d_{ij}}{\alpha_{ij}+b_{ij}-d_{ij}}\right)\right\} \quad \text{N} \tag{11}$$

where $\cos\phi_{ij} = \hat{r}_i\cdot\hat{r}_j$ and

$$b_{ij} = (\alpha_{ij}^2 - 2\alpha_{ij}\cos\phi_{ij} + 1)^{1/2}$$

$$c_{ij} = [2\alpha_{ij}(b_{ij} - \alpha_{ij} + \cos\phi_{ij})]^{1/2}$$

$$d_{ij} = [2\alpha_{ij}(b_{ij} + \alpha_{ij} - \cos\phi_{ij})]^{1/2} \tag{12}$$

When $\hat{r}_j$, $\hat{r}_j$ are nearly parallel, there is the small-angle approximation:

$$\vec{F}_{ij} = -\frac{\lambda_i\lambda_j a\alpha_{ij}}{\pi\epsilon_0 r_i}\left[\frac{\hat{r}_i\sin^{-1}\alpha_{ij}^{1/2}}{[\alpha_{ij}(1-\alpha_{ij})]^{1/2}} + \frac{\hat{r}_i - \hat{r}_j}{2(1-\alpha_{ij})}\left(1 + \frac{\sin^{-1}\alpha_{ij}^{1/2}}{[\alpha_{ij}(1-\alpha_{ij})]^{1/2}}\right)\right] \quad \text{N} \tag{13}$$

When $i=j$ this reduces to Eq. (5), with $Q=0$ and $R=r_i$.

For the general case of n line charges acting on a payload with charge Q,

$$\vec{F} = \frac{Q}{2\pi\epsilon_0}\sum_{i=1}^{n}\frac{\lambda_i\hat{r}_i}{r_i} + \sum_{i=1}^{n}\sum_{j=1}^{n}\vec{F}_{ij} \quad \text{N} \tag{14}$$

Let $\vec{e}$ be the force needed to remove a transverse velocity error. It then is necessary to have $\vec{F} = \vec{e}$. Taking any two independent $\vec{r}_i$ as a basis, there is uniquely

$$\vec{e} = \vec{F} = F_1\vec{r}_1 + F_2\vec{r}_2 \tag{15}$$

Since $\vec{e}$ is known, two components of $\vec{F}$ are to be specified and hence there are two unknowns among the λ_i. Hence $n-2$ of the λ_i may be arbitrarily specified; e.g., $(n-2)/2$ may be charged to potential $+V$ and $(n-2)/2$ to potential $-V$. From Eqs. (11, 14, 15) one writes

$$F_1 = \lambda_1 QA_1 + \lambda_1^2 B_{11} + \lambda_1\lambda_2 B_{12}$$

$$F_2 = \lambda_2 QA_2 + \lambda_2^2 B_{22} + \lambda_2\lambda_1 B_{21} \tag{16}$$

where the A_i and B_{ij} are functions of the selected basis $(\vec{r}_1, \vec{r}_2)$ through Eqs. (11, 12, 14). Equations (16) give two equations for the unknowns λ_1, λ_2 which resolve into a single quartic polynomial equation for either λ_1, λ_2.

C. Capacitance and System Performance

In standard capacitance formulas one assumes the capacitances are lumped and that the electric field within each capacitance is unperturbed by that of other nearby capacitances or conductors. In Fig. 2a these assumptions do not hold as there is an array of conductors giving rise to distributed fields which influence each other strongly. Hence one introduces the elastance tensor, following Smythe.[5] Let the rods be numbered 1 through n and let their associated potentials and line charge densities by V_i, λ_i, respectively: We have

$$(V_i) = (S_{ij})(\lambda_j) \qquad (\lambda_i) = (S_{ij})^{-1}(V_j) = (C_{ij})(V_j) \tag{17}$$

(V_i) is the vector $(V_1, V_2, \ldots, V_n)$; (λ_i) is $(\lambda_1, \lambda_2, \ldots, \lambda_n)$; (S_{ij}) and (C_{ij}) are $n\times n$ matrices of constant coefficients. (S_{ij}) is the elastance tensor. The element S_{mr} is the potential to which the rth rod is raised, when unit charge density is placed on the mth rod, all other rods being present but uncharged. $(C_{ij}) = (S_{ij})^{-1}$ is the tensor of capacitance or mutual inductance; the element C_{mr} is the ratio of the induced charge density on the rth rod to the potential of the mth rod when all rods, except the mth, are grounded. For all $m \neq r$, $S_{mr} = S_{rm}$, and $C_{mr} = C_{rm}$; also, $S_{mr} > 0$, $C_{mr} \leq 0$. C_{mm} is the self-capacitance of rod m and is the charge density-to-potential ratio when the other rods are present but grounded. Hence C_{mm} is not the same as the self-capacitance for an isolated conductor, as given in standard tables; however, $C_{mm} > 0$ always.

In general the S_{mr} must be found by experiment or by numerical solution of Laplace's equation. Nevertheless it is possible to present reference configurations which admit of analytical solution, for comparison with Eq. (1). Such configurations are modeled as linear dipoles.

1. *Parallel-Cylinder Capacitor*

In Fig. 2a, let all but two rods be deleted; these two rods are diametrically opposite, their centers being separated by $d_p = 2R$. The rod potentials are V, $-V$ and the payload of radius a also is at potential V. For rod radius r, the force on the payload is

$$F = \frac{8\pi\epsilon_0 a/d_p}{\cosh^{-1}(R/r)}V^2 = 222.53\frac{a/d_p}{\cosh^{-1}(R/r)} \quad \text{N/MV}^2 \tag{18}$$

The factor $1/\cosh^{-1}(R/r)$ then illustrates the performance/versatility tradeoff in comparing the parallel-plate corrector of Eq. (1) with the array of Fig. 2a.

2. *Single Rod with Surrounding Cylinder*

In Fig. 4 the array of Fig. 2a is surrounded by a grounded conducting cylinder, with radius P and clearance c beyond the outer periphery of the rods; hence $P = R + r + c$. We delete all rods save one; its capacitance with respect to the surrounding

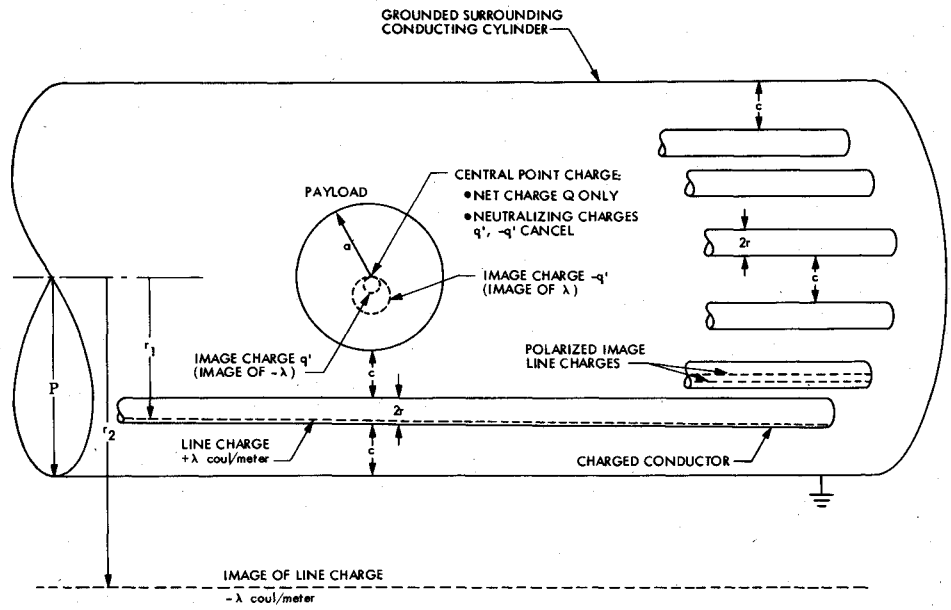

Fig. 4 Geometry of a charged sphere acted upon by a charged linear conductor enclosed within a grounded surrounding conducting cylinder.

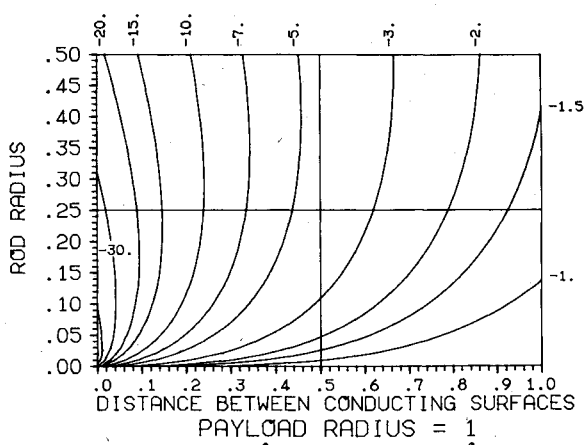

Fig. 5 Contour plot of F_λ/V^2, Eq. (21), in N/MV^2; abscissa and ordinate are respectively c/a and r/a.

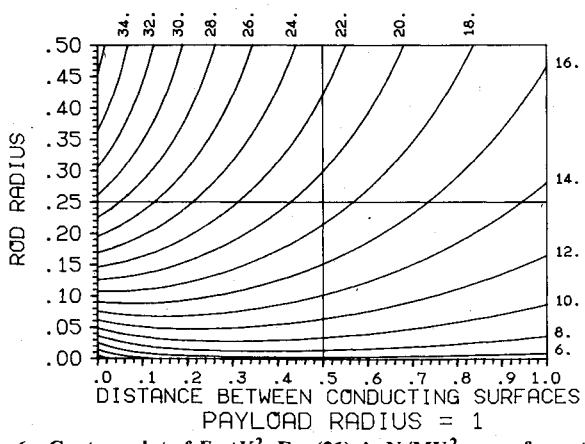

Fig. 6 Contour plot of F_Q/V^2, Eq. (21), in N/MV^2; same format as Fig. 5.

cylinder then is[4]

$$C=2\pi\epsilon_0/\cosh^{-1}[(P^2-R^2+r^2)/2Pr] \quad \text{F/m} \qquad (19)$$

In Fig. 4, both the charged rod surface and the surrounding cylinder are equipotentials of the linear dipole formed by the rod line charge λ and its image $-\lambda$. Hence λ is polarized outward from the rod centerline; its distance from the axis is $r_1=R+b$. The line charge image is at distance r_2 from the axis, where

$$r_1r_2=P^2 \qquad b(r_2-r_1+b)=r^2 \qquad (20)$$

Hence r_1, r_2 are roots of the quadratic,

$$Rr_i^2-(P^2+R^2-r^2)r_i+P^2R=0$$

The force on a payload due to the charged rod then is found from Eq. (13), since $\hat{r}_1$, $\hat{r}_2$ are coincident: $F=F_Q+F_\lambda$, where F is in newtons and

$$F_Q=(\lambda Q/2\pi\epsilon_0)(1/r_1-1/r_2)$$

$$F_\lambda=-\frac{\lambda^2a^2}{\pi\epsilon_0}\left(\frac{\sin^{-1}(a/r_1)}{r_1^2(1-a^2/r_1^2)^{1/2}}\right.$$

$$\left.-\frac{(r_1+r_2)\sin^{-1}[a/(r_1r_2)^{1/2}]}{(r_1r_2)^{3/2}(1-a^2/r_1r_2)^{1/2}}+\frac{\sin^{-1}(a/r_2)}{r_2^2(1-a^2/r_2^2)^{1/2}}\right) \qquad (21)$$

Also $\lambda=CV$, Eq. (19), and for a payload charged to potential V, $Q=4\pi\epsilon_0aV$. Figure 5 then is a contour plot of F_λ/V^2, Eq. (21), with V in megavolts. The ordinate is r/a and the abscissa is c/a; these normalized variables are equivalent to using r and c, with a taken as unity. The curves in Fig. 5 are contours of constant F_λ, in N/MV^2. Similarly, Fig. 6 is a contour plot of F_Q. We note that while the proximity of the rod and surrounding cylinder enhances C, the presence of the image line charge reduces the effectiveness of this configuration when compared to the parallel-cylinder capacitor of Eq. (18).

While one may often use dielectrics to reduce V in capacitors, this is not possible here. Dielectric polarization would introduce polarized image line charges which would effectively cancel those set up by the rods and their images.

III. Adjustment of Velocity Magnitude

A. Drift-Tube Theory

It has been suggested[3] that longitudinal fields be used for correction of velocity magnitude. However, these suggestions have gone no farther than to note the utility of "a series of drift tube electrodes stepped in voltage...developing about 3 kV/cm." Hence a preliminary treatment of this concept is in order.

The selected geometry (Fig. 7a) is a series of toroids, each of which is to be charged in succession as the payload passes down their channel. Each toroid has major radius R, and produces the field of a ring charge. The toroids have minor

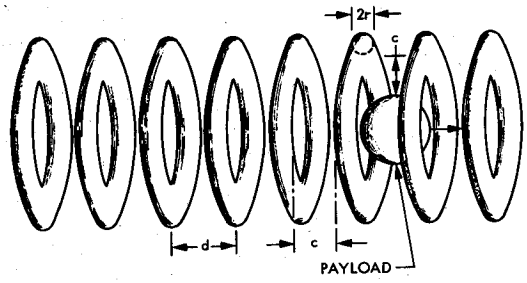

Fig. 7a Drift tube corrector with payload.

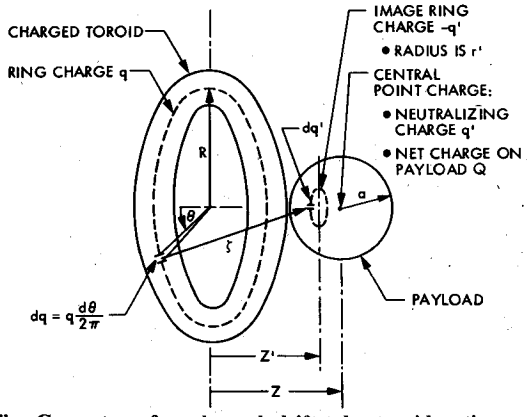

Fig. 7b Geometry of a charged drift-tube toroid acting upon a charged spherical coaxial payload.

radius r and clearance c between conducting surfaces; hence $d=c+2r$ and, as before, $R=r+a+c$, where a is payload radius.

Figure 7b illustrates the geometry of such a toroid acting upon a payload. Introduce cylindrical coordinates (ρ, z, θ) with origin at the toroid center and consider the potential $V(\rho, z, \theta)$. The toroid ring charge is q. With no loss of generality we take $\theta=0$. Also $\zeta=$distance to point (ρ, z, θ) from ring charge element $dq=(q/2\pi)d\theta$:

$$V(\rho,z)=\frac{1}{4\pi\epsilon_0}\int_{-\pi}^{\pi}\frac{1}{\zeta}\frac{dq}{d\theta}d\theta$$

$$=\frac{1}{4\pi\epsilon_0}\frac{q}{2\pi}\int_{-\pi}^{\pi}\frac{d\theta}{(\rho^2+R^2+z^2-2\rho R\cos\theta)^{1/2}}$$

$$=\frac{1}{4\pi\epsilon_0}\frac{q}{2\pi}\frac{4}{[(R+\rho)^2+z^2]^{1/2}}K(k)$$

$$k^2=\frac{4R\rho}{(R+\rho)^2+z^2} \tag{22}$$

where $K(k)$ is the complete elliptic integral of the first kind. For $R=0$ the toroid becomes a sphere and $V(\rho,z)=q/4\pi\epsilon_0(\rho^2+z^2)^{1/2}$, since $K(0)=\pi/2$.

For use in computing derivatives,

$$\frac{\partial k}{\partial z}=-\frac{zk^3}{4R\rho} \qquad \frac{\partial k}{\partial \rho}=\frac{k}{2\rho}\left(1-\frac{k^2}{2R}(R+\rho)\right)$$

$$\frac{dK(k)}{dk}=\frac{E(k)}{k(1-k^2)} \qquad \frac{dE(k)}{dk}=\frac{E(k)-K(k)}{k} \tag{23}$$

where $E(k)$ is the complete elliptic integral of the second kind. Hence there are the components E_ρ, E_z of the electric field $\vec{E}$:

$$E_\rho=-\frac{\partial V}{\partial \rho}=\frac{1}{4\pi\epsilon_0}\frac{q}{\pi}\frac{1}{\rho[(R+\rho)^2+z^2]^{1/2}}$$

$$\times\left[K(k)-\frac{R^2-\rho^2+z^2}{(R-\rho)^2+z^2}E(k)\right]$$

$$E_z=-\frac{\partial V}{\partial z}=\frac{z}{4\pi\epsilon_0}\frac{2q}{\pi}\frac{1}{[(R-\rho)^2+z^2][(R+\rho)^2+z^2]^{1/2}}E(k) \tag{24}$$

Near the axis, $\rho=d\rho\ll R$, one makes use of the expansions

$$K(k)=\frac{\pi}{2}\left(1+\frac{1}{4}k^2+\frac{9}{64}k^4+\cdots\right)$$

$$E(k)=\frac{\pi}{2}\left(1-\frac{1}{4}k^2-\frac{3}{64}k^4-\cdots\right) \tag{25}$$

and there are $E_{\rho 0}$, E_{z0}, being respectively the near-axial values of E_ρ, E_z:

$$E_{\rho 0}=\frac{1}{4\pi\epsilon_0}\frac{q}{2}\frac{2z^2-R^2}{(R^2+z^2)^{5/2}}d\rho$$

$$E_{z0}=\frac{z}{4\pi\epsilon_0}\frac{q}{(R^2+z^2)^{3/2}}$$

Let the payload center have coordinates $(\rho=d\rho, z=Z, \theta=0)$; there is no loss of generality in taking the off-axis displacement $d\rho$ to be in the direction $\theta=0$. From Eqs. (2), the image charge set up within the payload by ring charge q is a ring charge $-q'$. A line from the payload center to a point $(R, z=0, \theta)$ on q has length l: $l^2=R^2+Z^2-2Rd\rho\cos\theta$. A point on the image ring charge $-q'$ then lies at distance $l'=a^2/l$ from the payload center along the cited line of length l. Hence the image ring charge element $-dq'$ set up by dq has coordinates:

$$\rho=(l'/l)R[1+(2d\rho/R)(l/l'-1)\cos\theta]^{1/2}=\rho'+d\rho'$$

$$z=Z(1-l'/l)=Z'+dZ' \tag{27}$$

Now define $h=a^2/(R^2+Z^2)$ and Eqs. (27) are written,

$$\rho'=Rh \qquad d\rho'=d\rho[2(Rh/a)^2+1-h]\cos\theta$$

$$Z'=Z(1-h) \qquad dZ'=-d\rho[2RZ(h/a)^2]\cos\theta \tag{28}$$

Also the image ring charge density is

$$\frac{dq'}{d\theta}=\frac{q}{2\pi}h^{1/2}\left[1+\left(\frac{R}{a^2}\right)hd\rho\cos\theta\right] \tag{29}$$

and $q'=qh^{1/2}$. The payload carries at the center the neutralizing charge q', as well as net charge Q.

These developments permit treatment of two problems of payload motion.

1. Transverse Stability

We will now show it is almost always possible to select a value of Q such that the payload is restored toward the centerline under a transverse displacement. The electric field has the components of Eqs. (24). The force acting to move the payload transversely is F_ρ and one writes

$$\frac{dF_\rho}{d\rho}=\int_{-\pi}^{\pi}\left(E_\rho\frac{\partial}{\partial\rho}+\frac{\partial E_\rho}{\partial\rho}\frac{d\rho'}{d\rho}+\frac{\partial E_\rho}{\partial z}\frac{dz'}{d\rho}\right)\left(-\frac{dq'}{d\theta}\right)\cos\theta d\theta$$

$$+(Q+q')\frac{\partial E_{\rho 0}}{\partial\rho} \tag{30}$$

where $E_\rho = E_\rho(\rho,z)$ is evaluated for $\rho=\rho'$ and $z=Z'$, Eqs. (28). Also $E_{\rho 0}=E_{\rho 0}(z)$, Eq. (26), is evaluated for $z=Z$. Evaluating the integral,

$$\frac{dF_\rho}{d\rho} = -\frac{q'}{2}\left\{E_\rho\frac{Rh}{a^2}+\frac{\partial E_\rho}{\partial\rho}\left[2\left(\frac{Rh}{a}\right)^2+1-h\right]\right.$$
$$\left.-\frac{\partial E_\rho}{\partial z}\left(\frac{2RZh^2}{a^2}\right)\right\}+(Q+q')\frac{\partial E_{\rho 0}}{\partial\rho} \quad (31)$$

The stability criterion then is $dF_\rho/d_\rho<0$. Then $\partial E_\rho/\partial\rho$ and $\partial E_\rho/\partial z$ are given:

$$\frac{\partial E_\rho}{\partial\rho} = \frac{1}{4\pi\epsilon_0}\frac{q}{\pi}\frac{1}{\rho^2[(R+\rho)^2+z^2]^{1/2}}$$
$$\left\{\left(1+\frac{2\rho[(R^2-\rho^2)^2(R-2\rho)+2R(R^2+\rho^2)z^2+(R+2\rho)z^4]}{[(R-\rho)^2+z^2]^2[(R+\rho)^2+z^2]}\right)E(k)\right.$$
$$\left.-\left(1+\frac{2\rho^2z^2}{[(R-\rho)^2+z^2][(R+\rho)^2+z^2]}\right)K(k)\right\}$$

$$\frac{\partial E_\rho}{\partial z} = \frac{z}{4\pi\epsilon_0}\frac{q}{\pi}\frac{1}{\rho[(R+\rho)^2+z^2]^{3/2}[(R-\rho)^2+z^2]}$$
$$\left\{\left(\frac{(R^2-\rho^2)(R^2+7\rho^2)+2(R^2-3\rho^2)z^2+z^4}{(R-\rho)^2+z^2}\right)E(k)\right.$$
$$\left.-(R^2-\rho^2+z^2)K(k)\right\} \quad (32)$$

In Eqs. (32) one takes $\rho=\rho'$ and $z=Z'$, Eqs. (28), in obtaining coefficients for Eq. (31). One then defines Q_0 as the value of Q for which $dF_\rho/d\rho=0$

Figure 8 then shows Q_0/q as a function of Z/a, for six numbered values of R/a: $R/a=1.075$, 1.210, 1.345, 1.480, 1.615, 1.750, respectively. For any value of R/a, two stability regions are defined by the sign of $(2Z^2-R^2)$ in $E_{\rho 0}$, Eq. (26). For $Z^2<R^2/2$, $Q_0>0$ and stability exists for $Q>Q_0$; for $Z^2>R^2/2$, $Q_0<0$ and stability exists for $Q<Q_0$. In operational use one would charge the toroid during a specified range of Z/a, having an associated mean value of Q_0/q. The payload transverse oscillations would then be simple harmonic.

2. *Longitudinal Acceleration*

Let the payload and toroid be coaxial as in Fig. 7b; $d\rho=0$. The force on the payload then is $F_z=-q'E_z+(Q+q')E_{z0}$. Here $E_z=E_z(\rho,z)$, Eq. (24), with $\rho=\rho'$ and $z=Z'$, Eqs. (28); also $E_{z0}=E_{z0}(z)$, Eq. (26), with $z=Z$. Presented explicitly,

$$F_z = \frac{z}{4\pi\epsilon_0}\left(\frac{qQ}{(R^2+Z^2)^{3/2}}+\frac{q^2h^2}{a^3}u(R/a,Z/a)\right) \text{ N} \quad (33)$$

where

$$u(R/a,Z/a) = 1-\frac{1}{[(1-h)^2+(2hR/a)^2]^{1/2}}\frac{1}{1-h}\frac{2}{\pi}$$
$$\times E\left(\frac{2hR/a}{[(1-h)^2+(2hR/a)^2]^{1/2}}\right) \quad (34)$$

and $h=1/[(R/a)^2+(Z/a)^2]$. We then define the dimensionless influence function:

$$f(R/a,Z/a) = (Z/a)h^2u(R/a,Z/a)$$
$$q'(E_{z0}-E_z) = \frac{1}{4\pi\epsilon_0}\frac{q^2}{a^2}f(R/a,Z/a) \quad (35)$$

so that $f(R/a,Z/a)$ expresses the effect of the image charges.

In the limit $Z\to 0$, Eqs. (34, 35) become

$$\lim_{Z\to 0} f(R/a,Z/a) = \frac{Z}{a}h^2\left[1-\frac{1}{1-h^2}\frac{2}{\pi}E\left(\frac{2h^{1/2}}{1+h}\right)\right] \quad (36)$$

which is zero for $h=0.55303$. Hence for $R/a>1.3447$, $f>0$ for small Z/a. Figure 9 then gives $f(R/a, Z/a)$ for $0\le Z/a\le 4$

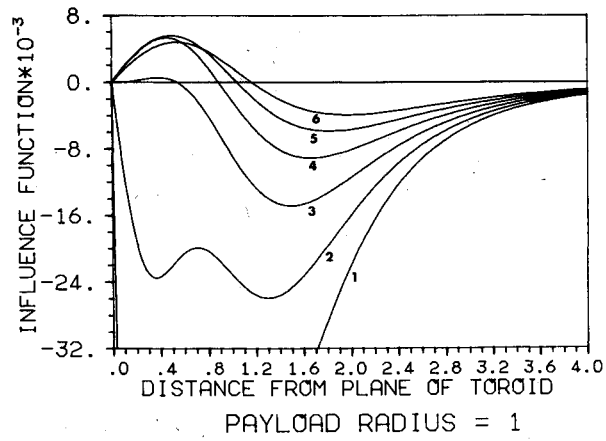

Fig. 9 Influence function $f(R/a, Z/a)$ Eq. (34,35), as a function of Z/a for $R/a=1.075$, 1.210, 1.345, 1.480, 1.615, 1.750, as numbered respectively.

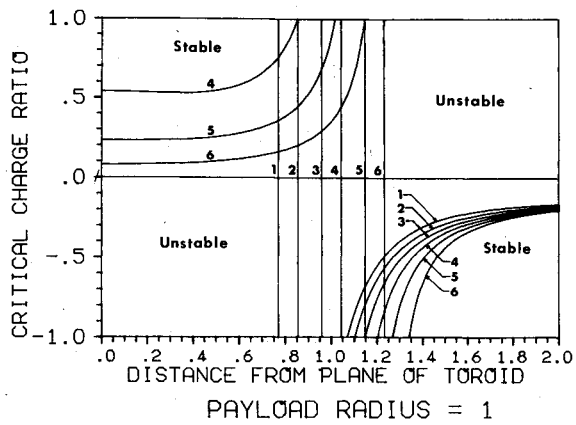

Fig. 8 Stability diagram for Eq. (31): Q_0/q, as a function of Z/a for $R/a=1.075$, 1.210, 1.345, 1.480, 1.615, 1.750, as numbered respectively.

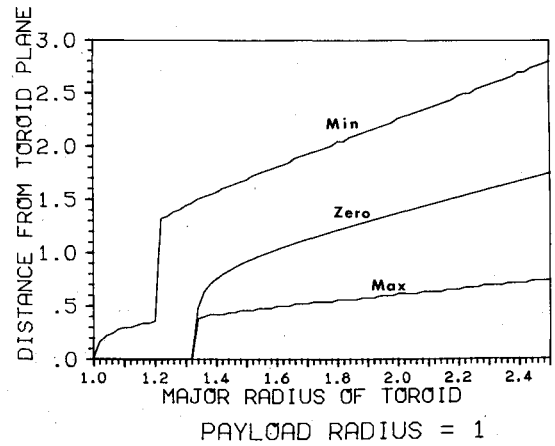

Fig. 10 Locations $(Z/a)_{\min}$, $(Z/a)_0$, $(Z/a)_{\max}$—respectively the minimum, zero, and maximum of $f(R/a,Z/a)$—as functions of R/a.

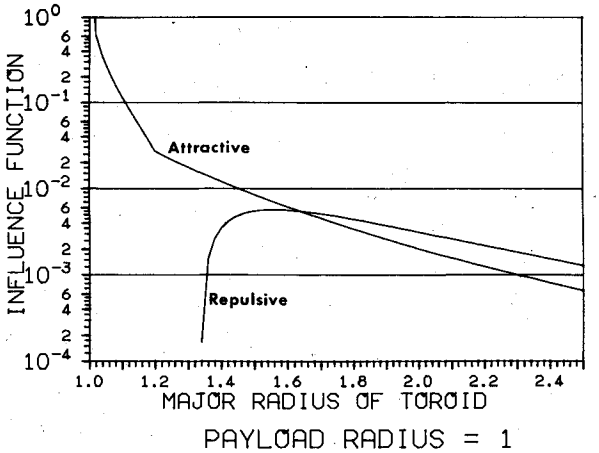

Fig. 11 Magnitudes of f_{att} and f_{rep}—respectively the minimum and maximum of $f(R/a,Z/a)$—as functions of R/a.

and for six values of R/a, these numbered values again being respectively 1.075, 1.210, 1.345, 1.480, 1.615, 1.750. Following the standard sign convention, the global minimum in such a curve corresponds to peak attraction on the payload; the global maximum corresponds to peak repulsion. Figure 10 then gives, as functions of R/a, the locations of the global minimum, the zero, and the global maximum of $f(R/a, Z/a)$. These locations we denote respectively $(Z/a)_{att}$, $(Z/a)_0$, $(Z/a)_{rep}$. The sudden jump in the curve of $(Z/a)_{att}$ near $R/a=1.2$ occurs because of a change in the relative magnitude of the two local minima illustrated by curve 2 of Fig. 9. The sawtooth behavior of the curves $(Z/a)_{rep}$, $(Z/a)_{att}$ results from the extrema being found by direct comparison of discretely computed function values, computed at intervals of 0.01 in Z/a. Finally, corresponding to $(Z/a)_{rep}$ and $(Z/a)_{att}$ are $f_{att}(R/a)=f[R/a,(Z/a)_{att}]$ and $f_{rep}(R/a)=f[R/a,(Z/a)_{rep}]$; these are given in Fig. 11 over the range $1\leq R/a\leq 2.5$, their curves being labeled respectively "attractive" and "repulsive." We have $f_{att}<0$, $f_{rep}>0$; hence Fig. 11 gives their magnitudes.

These developments are readily extended to the case of multiple toroids acting on a payload. Let n toroids so act, and define q_i as the ring charge on ith toroid; Z_i as the distance from ith toroid to payload center; Z_{ij} as the distance from ith toroid to image ring charge $-q_j'$ set up within the payload by the jth toroid. By extension of Eqs. (28),

$$h_j=a^2/(R^2+Z_j^2) \qquad Z_{ij}=Z_i-Z_jh_j$$
$$q_j'=q_jh_j^{1/2} \qquad r_j=h_jR \tag{37}$$

The force on the payload in newtons then is

$$F_z=\frac{Q}{4\pi\epsilon_0}\sum_{i=1}^{n}\frac{Z_iq_i}{(R^2+Z_i^2)^{3/2}}$$
$$-\frac{a}{4\pi\epsilon_0}\sum_{j=1}^{n}\frac{q_j}{(R^2+Z_j^2)^{1/2}}\sum_{i=1}^{n}q_i\left\{\frac{1}{[(R+r_j)^2+Z_{ij}^2]^{1/2}}\right.$$
$$\left.\times\frac{Z_{ij}}{(R-r_j)^2+Z_{ij}^2}\frac{2}{\pi}E\left[\left(\frac{4Rr_j}{(R+r_j)^2+Z_{ij}^2}\right)^{1/2}\right]-\frac{Z_i}{(R^2+Z_i^2)^{3/2}}\right\} \tag{38}$$

B. Capacitance and System Performance

By setting $V(\rho,z)=$const, Eq. (22) defines a family of toroidal equipotential surfaces, the limit $V\to\infty$ being the central ring charge. The toroid minor radius r in general then is not constant but is given by $r^2=(R-\rho)^2+z^2$. Thus r is approximately constant only for $r\ll R$. Hence to represent the field of a ring charge, the toroid of Fig. 7b must have a noncircular cross section defined implicitly by Eq. (22):

$$\frac{1}{[(R+\rho)^2+z^2)]^{1/2}}K\left[\left(\frac{4R\rho}{(R+\rho)^2+z^2}\right)^{1/2}\right]$$
$$=\frac{1}{2R-r}K\left(\frac{2[R(R-r)]^{1/2}}{2R-r}\right) \tag{39}$$

Equation (39) defines a closed curve $v(\rho,z)=w(R,r)=$const for specified r, R, where v and w are functions. Here we define $r=R-\rho$, with $z=0$; hence r is the distance between the ring charge and the circle of minimum ρ lying on the toroid. The capacitance of such a toroid then is

$$C=\frac{2\pi^2\epsilon_0(2R-r)}{K\{2[R(R-r)]^{1/2}/(2R-r)\}} \quad \text{F} \tag{40}$$

For $r\ll R$ there is the limit,

$$\lim_{k\to 1}K(k)=\ln[4/(1-k^2)^{1/2}]$$

Hence Eq. (40) gives the approximation

$$C\sim\frac{2\pi^2\epsilon_0(2R-r)}{\ln(8R/r-4)} \quad \text{F} \tag{41}$$

which is consistent with Ref. 4. Equation (41) is readily written in dimensionless variables R/a, r/a. In the cases treated here, $R/r\geq 3$ and Eq. (41) then introduces an error $\leq 0.68\%$ when compared to Eq. (40).

The presence of adjacent toroids increases C in accordance with the formalism of Eqs. (17) and it is desirable to account for this effect. An analytic expression is available by adaptation of Smythe's[5] discussion of the self-capacitance of two distant conductors. Here we consider only the effect of the nearest-neighbor toroid on either side. Let three consecutive toroids be numbered 1, 2, 3; we seek the self-capacitance C_{22} of toroid 2, which has charge q_2. Toroids 1 and 3 are at distance $d=c+2r$ to either side of 2. Hence the potential to which 1 and 3 are raised, from Eq. (22), is taken as

$$V_1=V_3\sim\frac{q_2}{4\pi\epsilon_0}\frac{1}{(R^2+d^2)^{1/2}} \quad \text{V} \tag{42}$$

which is $V(\rho,z)$ for $\rho=0$, $z=d$. Hence from Eqs. (17), $S_{21}=S_{23}=V_1/q_2$. Toroid 2 induces upon 1 (and 3) a charge polarization, so that the resulting field of 1 is a dipole field; but we ignore the change in the potential field at 2 due to the presence of this dipole field of 1 uncharged. Hence we take $S_{22}=V_2/q_2=1/C$ and similarly $S_{11}=S_{33}=1/C$, where C is Eq. (41). Finally, considering the effect of toroid 1 charged upon 2 and 3 uncharged, S_{13} is considered as given by Eq. (42) wherein one writes $2d$ for d. Thus, by ignoring all toroids except the nearest neighbors, and by ignoring potential-field perturbations due to charge polarization in these neighbors, one approximates the elastance tensor (S_{ij}):

$$\begin{bmatrix} S_{11} & S_{12} & S_{13} \\ S_{21} & S_{22} & S_{23} \\ S_{31} & S_{32} & S_{33} \end{bmatrix}= \tag{43}$$

$$\begin{bmatrix} 1/C & 1/4\pi\epsilon_0(R^2+d^2)^{1/2} & 1/4\pi\epsilon_0(R^2+4d^2)^{1/2} \\ 1/4\pi\epsilon_0(R^2+d^2)^{1/2} & 1/C & 1/4\pi\epsilon_0(R^2+d^2)^{1/2} \\ 1/4\pi\epsilon_0(R^2+4d^2)^{1/2} & 1/4\pi\epsilon_0(R^2+d^2)^{1/2} & 1/C \end{bmatrix}$$

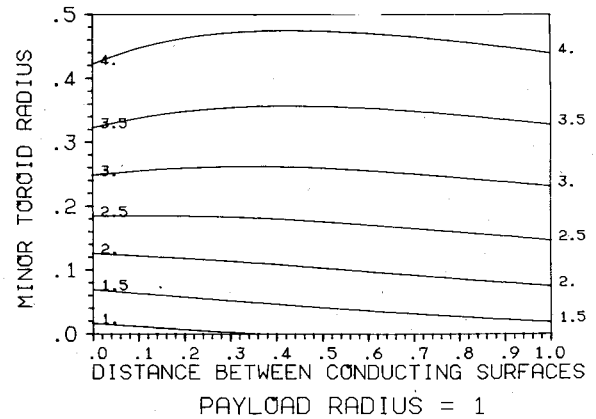

Fig. 12 Contour plot of normalized capacitance $C_{22}/4\pi\epsilon_0 a$, dimensionless; abscissa and ordinate are, respectively, c/a and r/a.

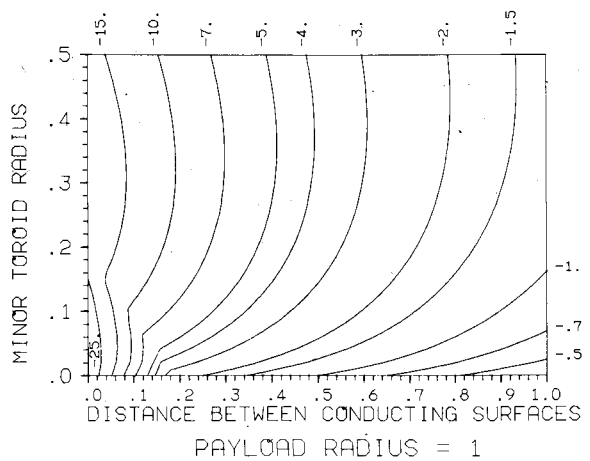

Fig. 13 Contour plot of $(F_{q'})_{att}/V^2$, Eq. (45), in N/MV^2; same format as Fig. 12.

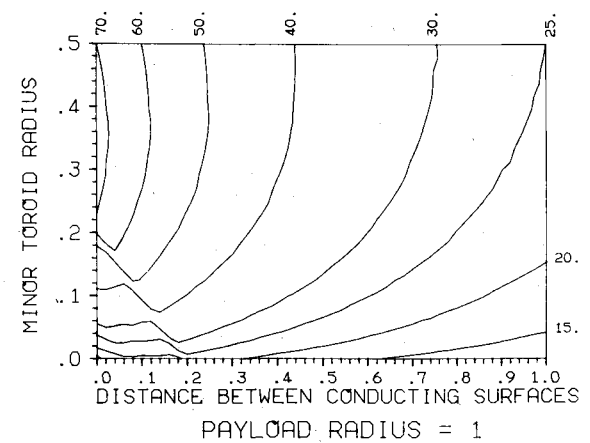

Fig. 14 Contour plot of $(F_Q)_{att}/V^2$, Eq. (45), in N/MV^2; same format as Fig. 12.

Then, taking account of the symmetry in Eq. (43),

$$C_{22} = \frac{S_{11}^2 - S_{13}^2}{S_{11}^3 - 2S_{12}^2(S_{11} - S_{13}) - S_{11}S_{13}^2} \tag{44}$$

which is found as the $(i=2, j=2)$ entry of $(S_{ij})^{-1}$. In Eqs. (42,43) one may write R/a, $d/a(=c/a+2r/a)$ for R,d; then in Eqs. (43,44), S_{ij} is replaced by $S_{ij}a$ and C_{22} is replaced by C_{22}/a. It then is possible to define a dimensionless capacitance $C_{22}/(4\pi\epsilon_0 a)$ which is the ratio of C_{22} to the capacitance of the payload. Figure 12 then plots contours of

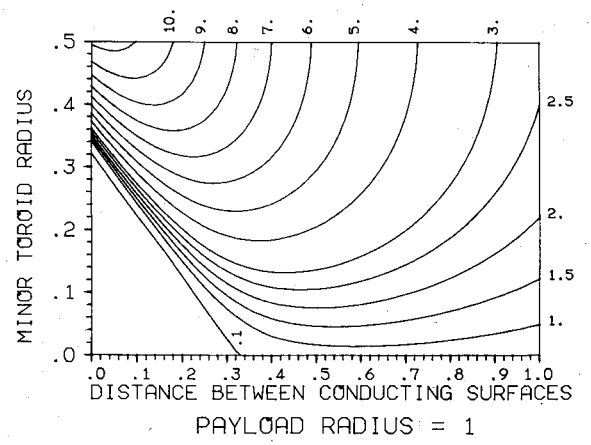

Fig. 15 Contour plot of $(F_{q'})_{rep}/V^2$, N/MV^2; same format Fig. 12.

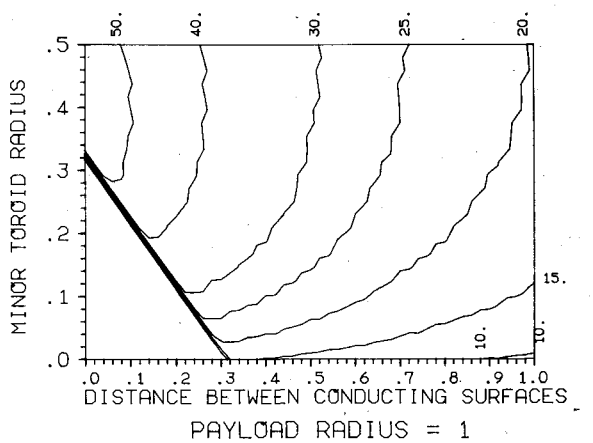

Fig. 16 Contour plot of $(F_Q)_{rep}/V^2$, N/MV^2; same format Fig. 12.

$C_{22}/(4\pi\epsilon_0 a)$, with the ordinate being r/a and the abscissa c/a. Since $R/a = 1 + r/a + c/a$, the geometry is completely defined for any point on the plot.

One now may obtain contour plots analogous to Figs. 5 and 6 given for transverse deflection. In Eqs. (33, 34) one has $q/a = (C_{22}/a)V$, $Q/a = 4\pi\epsilon_0 V$. Following Figs. 9-11, one also has $h_{att}(R/a) = 1/[(R/a)^2 + (Z/a)_{att}^2]$, where $(Z/a)_{att}$ is a function of (R/a) only; similarly there is h_{rep}. As in Eq. (21), we now write F_z, Eq. (33), as a sum of terms F_Q (from charge Q) and $F_{q'}$ (from the image charges), with F_Q and $F_{q'}$ being expressed as functions of r/a, c/a. In general there is also dependence on Z/a; hence we restrict attention to $(Z/a)_{att}$ and $(Z/a)_{rep}$. Then, for example, from Eqs. (33, 35),

$$(F_Q)_{att} = \left(\frac{Z}{a}\right)_{att} \frac{C_{22}}{a} h_{att}^{-3/2} V^2$$
$$(F_{q'})_{att} = f_{att} \frac{C_{22}}{a} \frac{C_{22}}{4\pi\epsilon_0 a} V^2 \tag{45}$$

and similarly for $(F_Q)_{rep}$ and $(F_{q'})_{rep}$, all of which are in newtons. Figure 13 then is a contour plot of $(F_{q'})_{att}/V^2$, in N/MV^2, plotted vs r/a and c/a in the format of Fig. 12. Similarly, Figs. 14-16 are contour plots respectively of $(F_Q)_{att}/V^2$, $(F_{q'})_{rep}/V^2$, $(F_Q)_{rep}/V^2$. In Fig. 15 the contour $(F_{q'})_{rep}/V^2 = 0.1$ delimits, very nearly, the region wherein in Fig. 10, $(Z/a)_{rep}$ fails to exist because $R/a < 1.3447$, as noted following Eq. (36). Since $F_z = F_Q + F_{q'}$, it is seen that if payload and toroid are charged to the same potential, F_z is approximately constant over the range from $(Z/a)_{rep}$ to $(Z/a)_{att}$.

IV. Considerations of High Voltage

Reasonable system performance involves velocity changes ~ 1 cm/s for corrector lengths < 100 m at lunar escape velocity, 2400 m/s. For payload masses $\sim$ 10 kg,[3] one requires $F_z \sim 5$ N and applied voltages are $V \sim 3 \times 10^5$ V. The same is true in transverse correction. Such high voltages raise the likelihood of electrical breakdown or arcing, a problem which is made more serious by the presence of lunar dust. Several aspects deserve comment.

1) Mechanism of breakdown initiation: It is well established[6] that for gap spacings $d_p \lesssim 0.1$ cm and $V \lesssim 100$ kV, breakdown is initiated by field-emission currents emanating from microscopic "whiskers" or protrusions, $\sim 10^{-4}$ cm in length, which extend even from very clean metal surfaces. These field-emitted electron currents may produce explosive evaporation of such a cathode protrusion owing to Joule heating, thus injecting an ionized microplasma into the gap. Alternately, for $d_p \sim 1$ cm,[7] the field-emission current may produce a localized electron-beam heating of the anode. For $d_p \gtrsim 1$ cm and $V \gtrsim 100$ kV, field-emission currents appear ineffective in triggering breakdown.[8,9] Instead, breakdown voltage $V_b \propto d_p^{1/2}$, approximately, and such breakdowns may be due to the Cranberg[10] mechanism. This involves macroparticles which adhere loosely to either electrode and which are detached by the applied electric field and accelerated across the gap, vaporizing upon impact.

2) Breakdown voltages: Summaries of experimental data on vacuum breakdown[6,10] indicate that over a range of at least $0.01 \leq d_p \leq 100$ cm, for clean, well-outgassed, and polished electrode surfaces of stainless steel or similar hard metals, the breakdown voltage is approximately

$$V_b = 3 \times 10^5 d_p^{1/2} \quad \text{V} \tag{46}$$

for d_p in centimeters. V_b may be increased by conditioning the electrode surfaces; this may involve their repeated subjection to sparking (breakdown) or to ion bombardment and sputtering. Alternately, V_b may be decreased by the presence of electrode surface contamination or dust, which encourages Cranberg breakdown.

3) Ambient dust: Dust, other than that which clings loosely to electrodes, may not be a direct source of problems. To see this, let a dust particle be spherical and of radius a; its mass is $m = (4/3)\pi\rho_{kg}a^3$, where ρ_{kg} = density. If the particle is uncharged ($Q = 0$), its dynamics are governed by Eq. (5) near a line charge. Letting x be the distance to the line charge,

$$\ddot{x} = \frac{F}{m} = -\frac{3\lambda^2}{4\pi^2\rho_{kg}\epsilon_0}\frac{1}{x^3} \quad \text{m/s}^2 \tag{47}$$

The first integral of Eq. (47) gives the kinetic energy per unit mass; also $\lambda = CV$ and $C \sim \pi\epsilon_0 V$. Then, for a dust particle initially at $x = \infty$, with $\dot{x} = 0$,

$$\frac{1}{2}\dot{x}^2 = \frac{3}{8}\frac{\epsilon_0 V^2}{\rho_{kg}x^2} \quad (\text{m/s})^2 \tag{48}$$

Let the charge-bearing rod have radius $r = 0.01$ m; let $V = 3 \times 10^5$ V, and take $\rho_{kg} = 2000$ kg/m^3. Then $\frac{1}{2}\dot{x}^2 = 1.49$ J/kg, an entirely inconsequential value showing that such a dust particle cannot pit surfaces or initiate breakdown by impact.

Such particles may gain or lose charge by any of several means. If a particle is near an anode, it may lose electrons by field emission from sharp microscopic points and, becoming positively charged, will be repelled. If it is near a cathode it cannot lose positive charge by field emission; but it may be the target of an electron beam field-emitted from a cathode protrusion. This electron bombardment may give the particle a negative charge, resulting in repulsion. It is also possible that the electron beam will heat the particle and produce thermionic electron emission, or that the beam will produce sputtering and evaporation of the particle, yielding a microplasma capable of initiating breakdown. However, Davies and Biondi[11] argue that repulsion from the cathode will occur for small Q.

4) Payload charging: One application in which electrical breakdown is useful is the charging of payloads. If an initially neutral payload passes close enough to an electrode at potential V, breakdown will occur and a dc current will flow onto the payload, continuing until charge transfer has raised the payload very nearly to potential V. Thus, for example, if the payload of radius a flies midway between equally charged parallel plates separated by distance d_p, it acquires charge Q (Ref. 4):

$$Q = \frac{4\pi\epsilon_0 V}{1/a - (2/d_p)\ln 2} \quad \text{C} \tag{49}$$

while if the payload flies down the centerline of a long cylinder of radius R,[4]

$$Q = 4\pi\epsilon_0 aV[1 - 0.8336a/R - 0.1024(a/R)^2 - 0.1757(a/R)^3 + 1.6946(a/R)(1 - a/R)^{-0.5463}] \quad \text{C} \tag{50}$$

If the charging electrode is maintained at potential V, the payload will gain kinetic energy in the amount QV upon leaving the electrode, due to repulsion.

A charged payload loses charge when exposed to the solar wind. If N is the number density of solar-wind protons or electrons, U_∞ their velocity, q_e their charge, b their impact parameter (radial distance over which they are drawn), and assuming all neutralizing ions stick to the payload and produce no secondary emission, the decay of payload charge Q is given:

$$\mathrm{d}Q/\mathrm{d}t = -\pi b^2 N U_\infty q_e \tag{51}$$

The payload potential is $V = Q/4\pi\epsilon_0 a$. The ions may be regarded as accelerated by an external potential V_∞; neglecting relativistic effects,

$$q_e V_\infty = \tfrac{1}{2} m_{e,p} U_\infty^2 \qquad b^2/a^2 = V/V_\infty \tag{52}$$

where $m_{e,p}$ is the mass of the electron or proton. Combining Eqs. (51,52),

$$\frac{\mathrm{d}Q}{\mathrm{d}t} = -\left(\frac{Nq_e^2 a}{2m_{e,p}\epsilon_0 U_\infty}\right)Q \tag{53}$$

The quantity in brackets is τ^{-1} where τ is the decay time constant. We have $q_e = 1.6 \times 10^{-19}$ C, $m_e = 9.1 \times 10^{-31}$ kg, and $m_p = 1836\, m_e$, and from Parker's[12] standard model of the solar wind, $N = (6 \pm 1) \times 10^6$ m^{-3}, $U_\infty = 4 \times 10^5$ m/s. Hence for a in meters, $\tau = 4.2 \times 10^{-5}/a$ s for electrons and $\tau = 0.77/a$ s for protons. In solar-storm conditions these values may be greatly reduced.

Hence, following charging, payloads in flight should be well shielded from the solar wind, as by a nonconducting tunnel. Evidently such a tunnel will be necessary for the downrange correctors; this tunnel will also aid in maintaining a dust-free environment. The charging of payloads will also contribute to this dust-free environment, which inhibits Cranberg breakdown. Payload charging will remove loose dust particles from their surfaces, and may aid as well in conditioning these surfaces.

Acknowledgments

It is a pleasure to acknowledge the support of Stanford University and its Department of Aeronautics and Astronautics, which provided facilities for the initial part of

this research. Other computational and graphics services were provided through the courtesy of the Jet Propulsion Laboratory. We have had valuable discussions with John Breakwell, Jim Stephens, and James Ary. This work represents one phase of research conducted at the Center for Space Science, with support from K.R.G., Inc.

References

[1] Von Herzen, B.P., "Light Pressure and Solar Wind Perturbations to Payload Trajectories,' in *Space Manufacturing Facilities III,* edited by J. Grey, AIAA, New York, 1979, pp. 599-501.

[2] Heppenheimer, T.A., "Guidance, Trajectory and Capture of Lunar Materials," in *Space Manufacturing Facilities III,* edited by J. Grey, AIAA, New York, 1979, pp. 473-490.

[3] Chilton, F., Hibbs, B., Kolm, H., O'Neill, G.K., and Phillips, J., "Mass-Driver Applications," in *Space-Based Manufacturing from Nonterrestrial Materials,* edited by G.K. O'Neill, Progress in Astronautics and Aeronautics, Vol. 57, AIAA, New York, 1977, pp. 63-94.

[4] Smythe, W.R. and Yeh, C., "Formulas," in *American Institute of Physics Handbook,* 3rd Ed., (D.E. Gray, coordinating editor) McGraw-Hill, New York, 1972, Chap. 5.

[5] Smythe, W.R., *Static and Dynamic Electricity,* McGraw-Hill, New York, 1968, pp. 36-38.

[6] Alpert, D., Lee, D.A., Lyman, E.M., and Tomaschke, H.E., "Initiation of Electrical Breakdown in Ultrahigh Vacuum," *Journal of Vacuum Science Technology,* Vol. 1, No. 1, Jan.-Feb. 1964, pp. 35-50.

[7] Utsumi, T., "Cathode- and Anode-Induced Electrical Breakdown in Vacuum," *Journal of Applied Physics,* Vol 38, No. 7, June 1967, pp. 2989-2997.

[8] Hawley, R., Zaky, A.A., and Eldine, M.E.Z., "Insulating Properties of High Vacuum," *Proceedings, IEE,* Vol. 112, No. 6, June 1965, pp. 1237-1248.

[9] Davies, D.K., "The Initiation of Electrical Breakdown in Vacuum—A Review," *Journal of Vacuum Science Technology,* Vol. 10, No. 1, Jan.-Feb. 1973, pp. 115-121.

[10] Cranberg, L., "The Initiation of Electrical Breakdown in Vacuum," *Journal of Applied Physics,* Vol. 23, No. 5, May 1952, pp. 518-522.

[11] Davies, D.K. and Biondi, M.A., "Mechanism of dc Electrical Breakdown between Extended Electrodes in Vacuum," *Journal of Applied Physics,* Vol. 42, No. 8, July 1971, pp. 3089-3107.

[12] Kennel, C.F. and Coroniti, F.V., "Jupiter's Magnetosphere," *Annual Review of Astronomy and Astrophysics,* Vol. 15, 1977, pp. 389-436.